

Overexpression and Mechanistic Characterization of Blastula Protease 10, a Metalloprotease Involved in Sea Urchin Embryogenesis and Development*

Received for publication, September 30, 2005, and in revised form, February 3, 2006. Published, JBC Papers in Press, February 21, 2006, DOI 10.1074/jbc.M510707200

Giordano F. Z. da Silva[‡], Rae L. Reuille[§], Li-June Ming^{†1}, and Brian T. Livingston^{§2}

From the Departments of [‡]Chemistry and [§]Biology, University of South Florida, Tampa, Florida 33620

Blastula protease 10 (BP10) is a metalloenzyme involved in sea urchin embryogenesis, which has been assigned to the astacin family of zinc-dependent endopeptidases. It shows greatest homology with the mammalian tolloid-like genes and contains conserved structural motifs consistent with astacin, tolloid, and bone morphogenetic protein 1. Astacin, a crustacean digestive enzyme, has been proposed to carry out hydrolysis via a metal-centered mechanism that involves a metal-coordinated “tyrosine switch.” It has not been determined if the more structurally complex members of this family involved in eukaryotic development share this mechanism. The recombinant BP10 has been overexpressed in *Escherichia coli*, its metalloenzyme nature has been confirmed, and its catalytic properties have been characterized through kinetic studies. BP10 shows significant hydrolysis toward gelatin both in its native zinc-containing form and copper derivative. The copper derivative of BP10 shows a remarkable 960% rate acceleration toward the hydrolysis of the synthetic substrate *N*-benzoyl-arginine-*p*-nitroanilide when compared with the zinc form. The enzyme also shows calcium-dependent activation. These are the first thorough mechanistic studies reported on BP10 as a representative of the more structurally complex members of astacin-type enzymes in deuterostomes, which can add supporting data to corroborate the metal-centered mechanism proposed for astacin and the role of the coordinated Tyr. We have demonstrated the first mechanistic study of a tolloid-related metalloenzyme involved in sea urchin embryogenesis.

The astacin family of zinc-dependent endopeptidases is ubiquitously distributed across all phyla and part of the superfamily of metzincins (1). Approximately 30 members of the astacin family have been characterized at the protein level (2), such as meprins, bone morphogenetic protein-1 (BMP-1),³ and tolloid, whereas several others have been identified through gene sequencing, including those in *Caenorhabditis elegans* (3). The signature of the sequence of the active site motif for this family of enzymes is HEXXHXXGXXH, where one Zn²⁺ ion coordi-

nates with the three histidines (boldface type), a tyrosine (Met-His/Ser-Tyr in a loop region downstream from the coordinated His residues), and a water molecule (4). Most members of this family share common domain structures such as the pre- and proenzyme sequences located immediately N-terminal to the protease domain. Several members contain one or two copies of epidermal growth factor (EGF)-like domains and complement-like domains (Clr, Cls) near the C terminus (2). The shuffling of different domains in relation to the catalytic protease domain creates a variety of proteins with different structures and functions.

Originally isolated and characterized as a developmentally regulated gene in sea urchin embryos (5, 6), the BP10 protein has remained uncharacterized. It shares sequence similarity with other members of the astacin family of enzymes (astacin itself being a crayfish digestive enzyme (4, 7) and hence a novel prototype in catalytic mechanism) important in development, such as tolloid-like and BMP-1 in vertebrates and tolloid in *Drosophila*. The BP10 protease is constructed of similar structural domains as BMP-1 and tolloid (*i.e.* astacin domain, CUB, and EGF) but has different arrangements and numbers of these domains. BP10 is most similar in sequence to the mammalian tolloid-like 2 proteins (8). The recent sea urchin genome sequencing project has revealed a cluster of genes homologous to BP10 (available on the World Wide Web at www.ncbi.nlm.nih.gov/Genomes/) as well as several related genes with similar structural domains. One of these, SpAN, has been implicated in regulating BMP-4 signaling (9). The transcription of the BP10 gene is transiently activated around the 16–32-cell stage, and the accumulation of BP10 mRNA peaks at the blastula stage. Temporarily, the highest BP10 activity is detected ~1.5 h after expression of the sea urchin hatching enzyme (envelysin) reaches a maximum (5). The BP10 transcripts are detected in a limited area of the blastula. The protein is first detected in late cleavage, and its level peaks in the blastula stage, declines abruptly before ingression of primary mesenchyme cells, and remains invariable in late development (5). Gache and co-workers (5) have proposed that BP10 acts as a zymogen activator, since an EGF domain is a highly conserved motif involved in proteolytic cascades or activation of precursors (5, 10), although its *in vivo* function is not yet known. Mammalian tolloid-like-2 proteins have been shown to process lysyl oxidase but not procollagen or chordin (11). In the sea urchin, blocking lysyl oxidase activity inhibits gastrulation (12, 13). Despite the uncertainty about its function, blocking BP10 activity prior to hatching with the use of an antibody resulted in abnormal embryos (5), reflecting the significance of this protease in embryo development.

BP10 has a unique arrangement of structural features (5, 6), such as the EGF-Ca²⁺ binding domain, two adjacent CUB domains, and a catalytic domain that is highly homologous to astacin. In particular, the EGF-Ca²⁺ domain is located between the catalytic domain and the proposed regulatory CUB sequences. More often, these EGF-

* This work was supported in part by National Science Foundation Grant 0296123 (to B. T. L.). The costs of publication of this article were defrayed in part by the payment of page charges. This article must therefore be hereby marked “advertisement” in accordance with 18 U.S.C. Section 1734 solely to indicate this fact.

¹ To whom correspondence may be addressed: Dept. of Chemistry, University of South Florida, 4202 E. Fowler Ave., Tampa, FL 33620. Tel.: 813-974-2220; Fax: 813-974-3203; E-mail: ming@shell.cas.usf.edu.

² To whom correspondence may be addressed: Dept. of Biology, University of South Florida, 4202 E. Fowler Ave., Tampa, FL 33620. Tel.: 813-974-7457; Fax: 813-974-3263; E-mail: blivings@cas.usf.edu.

³ The abbreviations used are: BMP, bone morphogenetic protein; Arg-NHOH, Arg-hydroxamate; BP10, blastula protease 10; LMCT, ligand-to-metal charge transfer transition(s); BAPNA, *N*-benzoyl-arginine-*p*-nitroanilide; TEMED, *N,N,N',N'*-tetramethylethylenediamine; EGF, epidermal growth factor; CAPS, 3-(cyclohexylamino)propanesulfonic acid; TAPS, 3-[[2-hydroxy-1,1-bis(hydroxymethyl)ethyl]amino]-1-propanesulfonic acid; MES, 4-morpholineethanesulfonic acid; NTA, nitrilotriacetic acid; PBS, phosphate-buffered saline.

Embryonic Blastula Protease 10 from Sea Urchin

Ca²⁺ domains are located between CUB sequences. CUB domains have been implicated in activity and regulation in BMP-1 (14). Astacin family enzymes and serine proteases have been implicated in remodeling the pericellular space in sea urchin embryos, which is composed of the extracellular matrix and transmembrane proteins (15, 16). Moreover, several studies have reported gelatinase and collagenase activities from enzymes located in the sea urchin egg and embryo, which were characterized as metalloenzymes due to inactivation with EDTA and 1,10-phenanthroline (17–20).

Besides the interesting distribution of astacin-like enzymes across phyla and the numerous functional roles of these enzymes in developmental biology, mechanistic questions about these highly conserved hydrolases domains still remain to be answered. Within the metzincin superfamily of enzymes, minor differences of active site function have been observed, which are likely to account for different substrate specificities (21). The metal-coordinated tyrosine in this protease family is a rather unusual metal-binding motif, due to possible reduction of Lewis acidity of the metal ion in the active site induced by the coordination of the negatively charged phenolate to the metal center (22, 23). However, the coordination of the Tyr-phenolate under physiological conditions does not seem to affect astacin catalysis under neutral conditions. The status of the coordinated tyrosine has been proposed to be an inhibitory process in the metal-centered hydrolysis of peptide bonds by astacin and serralsin (a bacterial metalloprotease containing an astacin-like active site) (24, 25). A metal-centered mechanism has been proposed for astacin and serralsin based on kinetic and spectroscopic studies of the enzymes and their Cu²⁺ derivatives (24, 25). In this mechanism, the active site Zn²⁺ coordinated by three His, a tyrosine, and a water molecule can be activated via detachment of the Tyr-phenolate with a concomitant deprotonation of the coordinated water assisted by a glutamate residue to afford the arrangement Zn²⁺–OH[–]•••Glu[–] without a coordinated Tyr. The metal-bound OH[–] is able to hydrolyze the scissile bond with Zn²⁺, creating electrostatic strain in the peptide bond by interaction with the carbonyl group of the scissile bond. To gain further insight into the mechanism of this family of developmentally significant proteases, we have performed and present herein the overexpression and thorough mechanistic study of recombinant BP10, which can serve as a model system for astacin-type developmentally regulated metalloenzymes. In this study, we show that BP10 is a zinc-dependent mononuclear metalloprotease with catalytic properties similar to astacin. Through the use of a synthetic substrate and porcine gelatin as substrates for the characterization of recombinant BP10, we demonstrate a unique Ca²⁺-dependent activation probably due to enhanced substrate binding. BP10 also is shown to have significant stability in the presence of chaotropic reagents by the use of circular dichroism. Finally, the copper derivative of BP10 is shown to have considerable catalytic and spectroscopic activities, which serve as evidence of the conserved astacin mechanism in developmentally regulated enzymes with the participation of the metal-coordinated tyrosine. Serralsin, a bacterial enzyme with similarity to BP10 only in the structure of the active site and in the primary sequence of the metal binding center, has similar substrate specificity.

Further analysis of BP10 will add insight into the catalytic mechanism of members of the astacin family and the degree to which the mechanism is conserved among the enzymes found in deuterostomes. Characterization of BP10 will also provide insight into the role of tollid family zinc endopeptidases in deuterostome development as well as the factors influencing substrate specificity of these enzymes.

EXPERIMENTAL PROCEDURES

Materials—The expression vector pQE30Xa, Ni²⁺-NTA-agarose, and mouse anti-His primary antibody were from Qiagen (Valencia, CA); XL1-Blue chemically competent *Escherichia coli* was from Invitrogen; Rosetta Blue chemically competent *E. coli* and Factor Xa removal kit were from Novagen (San Diego, CA); all primers were from Integrated DNA Technologies (Coralville, IA); all modifying and restriction enzymes were from Promega (Madison, WI); Eppendorf Perfect plasmid preparation was from Eppendorf (Westbury, NY); BM purple phosphatase substrate was from Roche Applied Science; EDTA, ZnCl₂, Cu(NO₃)₂, Ca(NO₃)₂, glycerol, ninhydrin, guanidine hydrochloride, bovine serum albumin, SDS, Triton X-100, Tween 20, imidazole, NaH₂PO₄, Na₂HPO₄, Tris-HCl, acrylamide, bisacrylamide, TEMED, ammonium persulfate, NaN₃, dimethyl sulfoxide (Me₂SO), sodium citrate, acetic acid, guanidine hydrochloride, and propanol were from Fisher; Type A porcine gelatin 300 bloom, *N*-benzoyl-arginine-*p*-nitroanilide (BAPNA), urea, isopropyl-β-thiogalactopyranoside, phenylmethylsulfonyl fluoride, benzamidine, urea, lysozyme, bicinchoninic acid, arginine-hydroxamate, and HEPES, CAPS, TAPS, and MES buffers were from Sigma; and 1,10-phenanthroline was from Acros (Fairlawn, NJ). All reagents were of enzyme or molecular biology grade when available, and all others were reagent grade. All glassware and plasticware were extensively rinsed with EDTA to remove metal contaminants and thoroughly washed with 18-megohm water to remove the chelator. All buffers contained Chelex resin to remove metal contaminants. CD spectra were collected in an AVIV 215 spectropolarimeter (Rheometric Scientific, Inc., Lakewood, NJ) at room temperature. All of the spectrophotometric measurements were performed in a Varian CARY 50 Bio-Spectrophotometer equipped with a PCB-150 water Peltier thermostable cell.

Overexpression, Purification, and Refolding of Recombinant BP1—The cDNA coding for *Paracentrotus lividus* BP10 cloned into the pBluescript plasmid (pBP10) was a generous contribution from Christian Gache and Thierry Lepage (Unité de Biologie Cellulaire, Center National de la Recherche Scientifique et Université de Paris VI, Station Marine, Villefranche-sur-Mer, France). PCR primers coding for both 5' and 3' regions were designed according to the proposed full-length BP10 to subclone the cDNA into the pQE30Xa overexpression vector. The 5' primer (5'-PO₄-AAACTA-ATACTTCCCTTTCGGGATTG-3') codes for the first nine codons in the proposed nucleotide sequence in BP10 and is 5'-phosphorylated for blunt end cloning using the *Stu*I restriction site in pQE30Xa; 3' primer was designed for cloning into the *Xma*I restriction site 5'-**AATCCCCGGGT-TAGTT**CAGACGAGGATCTCGGGT-3' (where the boldface type represents extra base pairs for melting temperature optimization, the underline represents the *Xma*I restriction site, and underlined boldface type represents the stop codon). The PCR product coding for BP10 was digested with *Xma*I and cloned into the pQE30Xa vector. The BP10 construct was transformed into Rosetta Blue competent cells. The colonies overexpressing recombinant BP10 were screened using a colony lift protocol according to Qiagen without modifications, where the production of BP10 was monitored using a mouse anti-His tag primary antibody. The active colonies were picked, propagated in liquid medium to A₆₀₀ = 0.4. Isopropyl-β-thiogalactopyranoside was added to a final concentration of 1.0 mM, and the culture was grown at 30 °C and 300 rpm for 4.5 h. The bacteria containing recombinant BP10 were pelleted at 4000 × *g* at 4 °C and resuspended in cell wall lysis buffer (50.0 mM NaH₂PO₄, 100.0 mM NaCl, 10.0 mM imidazole, 2.0 mM benzamidine, 2.0 mM phenylmethylsulfonyl fluoride, pH 8.0) containing 1.7 mg/ml lysozyme, incubated on ice lightly shaking for 60 min, and then sonicated for 6 × 10 s with 10-s intervals. The cultures were pelleted at 10,000 × *g* at 4 °C for 20 min, and the inclusion bodies were resuspended in

a urea buffer (8.0 M urea, 10.0 mM Tris, 100.0 mM NaH_2PO_4 , 1.0% Triton X-100, 2.0 mM benzamidine, 2.0 mM phenylmethylsulfonyl fluoride, pH 8.0) and incubated at 37 °C at 200 rpm for 60 min. The solubilized inclusion bodies were pelleted at $10,000 \times g$ at 4 °C for 20 min, and 1.0 ml of Ni^{2+} -NTA-agarose was added to the supernatant. The Ni^{2+} -NTA slurry was gently shaken at room temperature for 45 min and then added to a gravity-fed column, and the recombinant BP10 was eluted using a pH gradient, with buffers containing 6.0 M urea, 10.0 mM Tris, 100.0 mM NaH_2PO_4 , at pH values of 6.3, 5.9, and 4.5. The recombinant BP10 was completely eluted at pH 4.5 and was immediately titrated to pH 7.4 using 0.5 M NaH_2PO_4 . Overexpression and purification were monitored on a time-dependent basis using 12.5% SDS-PAGE according to Laemmli and Western blot techniques using the anti-His tag antibody.

The concentration of recombinant BP10 was determined using standard BCA assay with a bovine serum albumin standard curve. The recombinant protein was diluted 40 times by volume using 50.0 mM Tris with 50 mM NaCl and then dialyzed extensively with several changes against phosphate-buffered saline (PBS) containing 50 μM ZnCl_2 for 48 h at 4 °C. Recombinant BP10 was concentrated under 18 p.s.i. N_2 using either an YM3 Amicon membrane or an Amicon Centricon YM3 spin column. Final BP10 concentrations were checked using BCA. The His tag fusion was removed using a Factor Xa His tag removal kit from Novagen according to the manufacturer's instructions.

Preparation of the Copper Derivative of BP1—During the refolding of urea-denatured BP10, 1.0 mM 1,10-phenanthroline was added to the 50.0 mM Tris, 50.0 mM NaCl, pH 7.5 buffer and then extensively dialyzed against PBS containing 0.5 M guanidine-HCl. The guanidine-HCl-containing buffer was exchanged through dialysis with PBS buffer and then with PBS containing 50 μM $\text{Cu}(\text{NO}_3)_2$. Protein concentrations were determined with BCA assay.

CD Studies—CD spectra of urea-denatured and folded Zn-BP10 and Cu-BP10 were collected in PBS using a 0.1-cm cell with a resolution of 0.5 nm. All absorbance readings were converted to molar ellipticity, and the α -helical content was calculated according to published methods (26).

Gelatin Zymogram—Gelatin was incorporated into a polyacrylamide gel matrix according to standard protocols with modifications to fit current studies as described below (27). A volume of 1.25 ml of 1.4 M Tris at pH 8.8, 0.50 ml of 5.0 mg/ml gelatin solution in water, 25.0 μl of 10% (w/v) ammonium persulfate, 200 μl of 10% (w/v) SDS, 25.0 μl of TEMED, 2.0 ml of water, and 1.25 ml of 30:1 acrylamide/bisacrylamide were mixed and allowed to polymerize in a minigel minus a stacking gel. Several concentrations of BP10 were mixed with nonreducing gel-loading dye and incubated for 15 min at room temperature (standard Laemmli protocol minus mercaptoethanol or dithiothreitol (28)). These BP10 samples were loaded into each lane of the gel and run at 200 V and 4 °C until the dye front reached the bottom of the plate. The running buffer did not contain SDS. The gel was washed two times in 0.25% Triton X-100 for 15 min with gentle shaking and then incubated for 10 h in 50.0 mM Tris, pH 7.50, 1.0 μM ZnCl_2 , 0.5% Triton X-100, 0.02% NaN_3 , and 2.0 mM CaCl_2 . After 10 h, the gels were stained with 0.1% Coomassie Brilliant Blue in 40% propanol for 1.0 h. The gel was destained in a 7% acetic acid solution to reveal the digestion and then photographed on a light table with a digital camera.

Gelatinase Assay—The gelatinase activity of recombinant BP10 was monitored using a detection method for α -amino groups with ninhydrin as an indicator of peptide hydrolysis according to a standard protocol with modifications to fit current studies as described below (29). A 5.0 mg/ml gelatin solution was prepared in H_2O and heated to 55 °C for 15 min until completely dissolved. A ninhydrin detection solution was

prepared by mixing 9.0 ml of glycerol, 3.0 ml of 0.5 M sodium citrate at pH 5.50, and 3.75 ml of 1.0% (w/v) ninhydrin solution in 0.5 M sodium citrate buffer. Gelatin and BP10 (1.0 μM final concentration) were mixed in PBS and incubated at room temperature. A 50.0- μl sample was taken from the reaction at several time points and mixed with 950 μl of ninhydrin detection solution and then boiled for 12.0 min; then the absorbance at 570 nm was determined. A sample containing undigested stock gelatin (the same gelatin used for the experiment, incubated under the same conditions without BP10) mixed with the same detection assay was used as the blank. The pseudo-first-order rate constant k_{obs} was determined from an exponential curve fit. The molar absorptivity of Ruhemann's purple ($\epsilon_{570} = 22,000 \text{ M}^{-1} \text{ cm}^{-1}$) (30) was used to determine gelatin concentrations in millimolar and also allowed for monitoring the substrate-dependent hydrolysis of gelatin. Several dilutions of a 10.0 mg/ml stock solution of gelatin incubated with BP10 with time points taken at 0.0, 2.0, 4.0, 8.0, and 16.0 min were used to calculate the initial rate using the ninhydrin detection method described above. Initial rates were fitted as a function of substrate concentration according to the Michaelis-Menten equation, yielding k_{cat} and K_m parameters.

Hydrolysis of BAPNA by Zn-BP10 and Cu-BP1—BAPNA stock solutions were made in Me_2SO and then diluted with 50.0 mM HEPES, 50.0 mM NaCl, pH 7.50. Less than 2% Me_2SO by volume was present in each assay and found not to interfere with kinetic measurements. Several concentrations of BAPNA were incubated with 2.17 μM BP10, and rates were determined colorimetrically from the release of the *p*-nitroaniline product ($\epsilon_{405} = 10,150 \text{ M}^{-1} \text{ cm}^{-1}$). Kinetic parameters were determined by nonlinear fitting to the Michaelis-Menten equation.

Calcium Activation Assays—Gelatin was extensively dialyzed against an EDTA solution and then extensively dialyzed to remove the chelator. Calcium was carefully titrated under substrate saturation conditions to determine its effect on the hydrolysis of gelatin and BAPNA. Once saturating concentrations of calcium were determined, new kinetic parameters were obtained using sufficient (1.0 mM) calcium in all buffers.

Inhibition Studies—The effects of two inhibitors, 1,10-phenanthroline and arginine-hydroxamate (Arg-NHOH), on the hydrolysis of BAPNA were determined by running Michaelis-Menten kinetics under several concentrations of each inhibitor. Inhibition constants were determined according to the inhibition patterns for 1,10-phenanthroline and Arg-NHOH, respectively.

pH Profiles—The pH profiles for Zn- and Cu-BP10 catalysis were constructed by monitoring gelatin and BAPNA hydrolysis under several different pH values using 50.0 mM buffers containing 50.0 mM NaCl and 1.0 mM CaCl_2 . The following buffers were used: acetate (pH 5.0), MES (pH 5.5–6.5), HEPES (pH 7.0–8.0), TAPS (pH 8.5–9.0), and CAPS (pH 9.5–11.0). The pH-dependent kinetic parameters were determined by nonlinear fitting to the Michaelis-Menten equation, and $\text{p}K_a$ values were obtained from fitting the kinetic parameters to a two-ionization process.

Electronic Spectrum of Cu-BP1—The electronic spectrum of 20.0 μM Cu-BP10 was obtained from 350 to 800 nm, and the tyrosine to copper charge transfer transition was observed at 454 nm. The quenching of this ligand-to-metal charge transfer transition (LMCT) was monitored spectrophotometrically upon the addition of Arg-NHOH.

RESULTS AND DISCUSSION

Overexpression and Refolding of Recombinant BP1—The recombinant enzyme was efficiently overexpressed, although it was insoluble and contained within inclusion bodies (Fig. 1, lane 3). Urea solubilization proved to be an efficient method for extracting the enzyme from

Embryonic Blastula Protease 10 from Sea Urchin

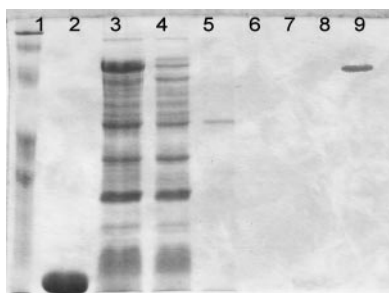


FIGURE 1. SDS-polyacrylamide gel (12.5%) during purification of recombinant BP10. Lane 1, molecular mass marker (200, 97.4, 66.2, 45, and 31 kDa from the top); lane 2, total soluble protein after 4 h induction after lysozyme and sonication; lane 3, total protein solubilized with 8.0 M urea from inclusion bodies; lane 4, flow-through unbound proteins from Ni²⁺-NTA column; lanes 5 and 6, buffer C wash; lanes 7–9, buffer D at pH 6.3, 5.9, and 4.5 gradient elution, respectively. Lane 9 shows a homogenous band at 66 kDa, assigned to recombinant BP10.

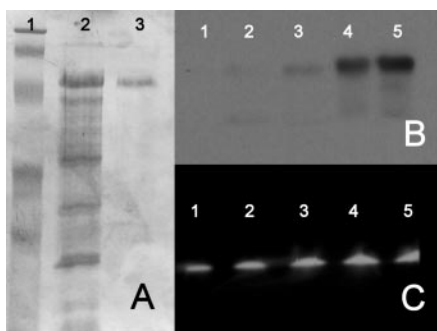


FIGURE 2. A, SDS-PAGE (12.5%) of intact BP10 after refolding. Lane 1, molecular mass marker (200, 97.4, 66.2, 45, and 31 kDa from the top); lane 2, total urea-solubilized protein; lane 3, recombinant BP10 after refolding. **B,** Western blot for the time course of overexpression. Lane 1, uninduced sample; lanes 2–5, 1.0, 2.0, 3.0, and 4.0 h, respectively. **C,** gelatin zymogram for concentration-dependent substrate hydrolysis by BP10; lanes 1–5, 0.25, 0.50, 1.0, 1.50, and 1.75 μM BP10, respectively.

inclusion bodies, coupled with a fusion His tag at the N terminus to BP10 that allows for efficient purification using Ni²⁺-NTA-agarose. The overexpression and purification yields an average of 0.7 mg/ml total recombinant BP10 after a pH gradient elution from the Ni²⁺-NTA-agarose column (Fig. 1). The protein overexpression was monitored on a time course using SDS-PAGE and Western blotting (Fig. 2B). The detection of the His tag using an anti-His antibody upon induction with isopropyl-β-thiogalactopyranoside proved a sensitive and consistent method for monitoring the overexpression of the recombinant protein.

Upon removal of the chaotropic reagent urea through extensive dialysis, the protein was refolded, and activity could be monitored after removal of the His tag. It was determined empirically that a 40-fold dilution of the denatured protein prior to dialysis was important, since at higher concentrations, the protein coagulates and precipitates out of solution. Due to the large number of cysteine residues in BP10, cysteine and reduced glutathione were included in the refolding process in separate attempts. However, this refolding process yielded inactive protein. The use of oxido-shuffling reagents, oxidized/reduced glutathione, or cysteine/cystine during refolding was also attempted without success. Stabilization of folding intermediates using a smaller concentration of guanidine HCl and L-arginine to improve solubility proved to be the most efficient method of refolding and keeping the protein soluble (31).

The CD spectrum of urea-denatured BP10 (Fig. 3, dotted trace) does not show features at 195 (negative) and 220 (slightly positive) nm for random coil expected in the presence of a high concentration of chaotropic reagents but shows overall β-sheet-predominant features with blue shifts observed in the minimum and a red shift in the maximum of the spectrum. This resistance to complete denaturation to a random

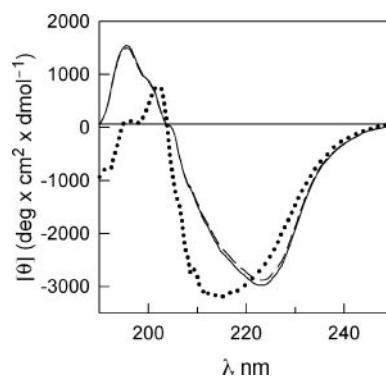


FIGURE 3. CD spectra of Zn-BP10 in PBS with 8.0 M urea, pH 7.4 (dotted trace), and renatured Zn- (solid trace) and Cu-BP10 in PBS, pH 7.4 (dashed trace).

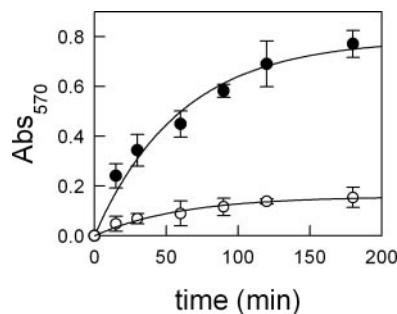


FIGURE 4. First order kinetics of gelatin hydrolysis by Zn²⁺ (●) and Cu²⁺ (○) derivatives of BP10 in the presence of 1.0 mM Ca²⁺ at pH 7.5. The solid traces are the best fit to a pseudo-first-order rate law, which affords the rate constant k_{obs} for each derivative.

coil conformation due to partially formed secondary structure may account for the efficient refolding of BP10 in the absence of reducing agents. The helical content of BP10 is calculated to be 5.76% on the basis of the CD (26), which is consistent with the large content of sheet-like structures (*i.e.* β-barrel) in CUB domain-containing proteins (32). According to sequence homology, only the helices present in the astacin domain should account for the low helical content of BP10, which would yield a helical content of 6.86%, which is consistent with observations from the CD spectrum. The CD spectra of Zn-BP10 and Cu-BP10 are virtually identical (*solid* and *dashed* traces in Fig. 3), suggesting no major conformational change in the overall structure of the protein due to metal substitution.

Recombinant BP10 showed no signs of degradation after refolding (Fig. 2A). Upon removal of the His tag using a Factor Xa removal kit from Novagen, the protein undergoes autohydrolysis and remained stable only for a few days at 4 °C. However, the protein fused with the His tag is stable indefinitely at 4 °C. Hence, the His tag was used as an efficient method for long term storage of recombinant BP10 and removed only prior to running experiments.

Kinetics of Gelatin Hydrolysis—Recombinant BP10 was not able to hydrolyze casein, a commonly used substrate for endopeptidases. Porcine gelatin, however, proved to be a good substrate to monitor proteolytic activity of BP10 with gelatin zymograms (Fig. 2C) and a ninhydrin detection protocol (Figs. 4 and 5), establishing the proposed role of BP10 as a protease. The formation of a colored ninhydrin-α-amino acid conjugate with a known molar absorptivity was a convenient method to monitor gelatin hydrolysis, from which a pseudo-first-order kinetics can be established, and the observed rate constant k_{obs} was determined to be 0.02 s⁻¹ under saturating conditions of 5.0 mM gelatin (Fig. 4). The initial rates for the hydrolysis of gelatin at different concentrations were determined, which reached saturation at gelatin concentration greater than 0.5 mM. The saturation kinetics can be fit to the Michaelis-Menten

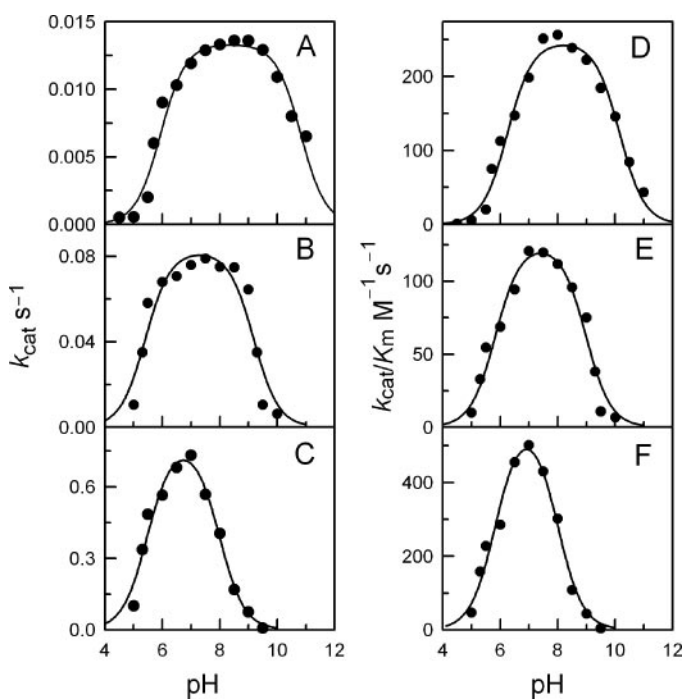


FIGURE 5. pH dependence of k_{cat} and k_{cat}/K_m for the hydrolysis of gelatin by Zn-BP10 (A and D), hydrolysis of BAPNA by Zn-BP10 (B and E), and hydrolysis of BAPNA by Cu-BP10 (C and F). The solid traces are the best fit to the equation, $k = k_{lim}/((1 + [H^+]/K_{a1})(1 + K_{a2}/[H^+]))$ to afford the two pK_a values reported here.

equation to yield $k_{cat} = 0.013 \text{ s}^{-1}$, $K_m = 51.3 \text{ }\mu\text{M}$, and the second-order rate constant $k_{cat}/K_m = 253 \text{ M}^{-1} \text{ s}^{-1}$ (Fig. 5). Interestingly, BP10 shows a significant Ca^{2+} -dependent activation (Fig. 4, inset), yielding $k_{cat} = 0.77 \text{ s}^{-1}$, $K_m = 46.5 \text{ }\mu\text{M}$, and $k_{cat}/K_m = 16,740 \text{ M}^{-1} \text{ s}^{-1}$ at $[\text{Ca}^{2+}] > 0.05 \text{ mM}$. From the dependence of the activity with $[\text{Ca}^{2+}]$, an affinity constant of 83.3 mM^{-1} can be obtained for Ca^{2+} binding to BP10 that is important for the nonessential activation of the enzyme. Other gelatinases found in the sea urchin embryos have shown a Ca^{2+} -dependent activation (33, 34). However, whether or not the Ca^{2+} bound to the EGF domain is a cofactor also involved in protein-protein interaction or signaling besides enhancing the activity is not known for BP10 and cannot be determined in these studies. Further analysis of the rate constants can provide insight into the role of Ca^{2+} in catalysis. The K_m values are similar in the presence and absence of Ca^{2+} , whereas the k_{cat} value for the catalysis in the presence of Ca^{2+} is 60-fold larger than in the absence of Ca^{2+} . Since K_m is defined as $(k_{-1} + k_{cat})/k_1$, with k_1 and k_{-1} the rate constants for substrate binding and dissociating from the enzyme-substrate (ES) complex, a significant increase in k_{cat} with a constant K_m value in the presence of Ca^{2+} reflects a decrease in dissociation constant k_{-1}/k_1 of the ES complex. This observation reveals that Ca^{2+} affects BP10 catalysis by enhancing substrate binding to the enzyme and by lowering the activation energy (*i.e.* a larger k_{cat} value). The activation of BP10 by Ca^{2+} is the first report of the effect of Ca^{2+} on the activity of astacin family metalloproteases. The lighter alkaline earth metal Mg^{2+} showed no effect in activation of BP10. BP10 contains an EGF- Ca^{2+} domain that could mediate the effect of calcium on catalysis. Elucidation of the roles of the EGF domain and Ca^{2+} on BP10 activity may shed insight on the action of other structurally conserved enzymes, particularly when these enzymes have been characterized across all phyla.

The kinetic parameters for Zn-BP10 toward gelatin hydrolysis were determined between pH values 4.5 and 11.0. Plots of k_{cat} and k_{cat}/K_m against pH exhibit bell-shaped curves (Figs. 6, A and D), indicating the

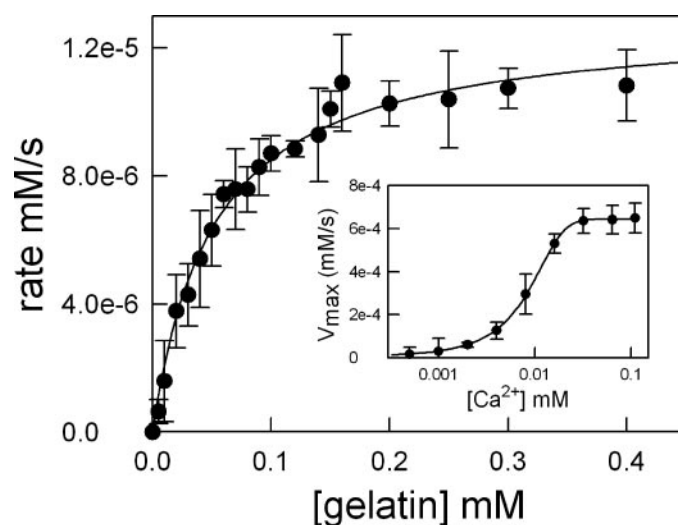


FIGURE 6. Gelatin hydrolysis by $1.0 \text{ }\mu\text{M}$ Zn-BP10 in 50.0 mM HEPES, pH 7.5, 50 mM NaCl, and 1.0 mM $\text{Ca}(\text{NO}_3)_2$. The solid curve is the best fit to the Michaelis-Menten equation. The inset shows a Ca^{2+} -dependent activation upon titration of Ca^{2+} to $60 \text{ }\mu\text{M}$ Zn-BP10. The solid curve in the inset is a best fit to a 1:1 ligand/metal binding pattern.

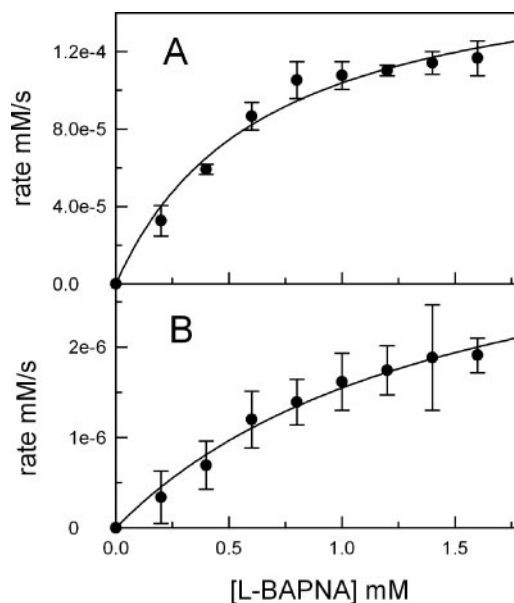


FIGURE 7. A, hydrolysis of L-BAPNA by Zn-BP10 in 50.0 mM HEPES, pH 7.5, in the presence of 50 mM NaCl, and 1.0 mM $\text{Ca}(\text{NO}_3)_2$. B, same as in A in the absence of Ca^{2+} .

presence of two ionizable groups in the catalytic mechanism of Zn-BP10. Two ionization constants, $pK_{a1} = 5.94$ and $pK_{a2} = 10.2$, were obtained from the k_{cat} versus pH profile, and $pK_{a1} = 6.3$ and $pK_{a2} = 10.1$ were obtained from the k_{cat}/K_m versus pH profile, which can be assigned to the deprotonation of a zinc-bound water and the coordinated tyrosine, respectively, which are consistent with previous reports for serralyisin (24). The role of the coordinated Tyr in BP10 catalysis is further addressed below.

Kinetics of BAPNA Hydrolysis—The synthetic peptide mimic BAPNA is a good substrate for BP10. This activity was previously observed for serralyisin, but not astacin, and is the only synthetic tripeptide of a series of di- and tripeptide mimics, including Gly-, Ala-, Val-, Leu-, Glu-, Lys-, Arg-, Ala₃-, and succinyl-Ala₃-*p*-nitroanilide, that was hydrolyzed by BP10. The kinetics of BAPNA hydrolysis follows Michaelis-Menten kinetics (Fig. 7A) to yield $k_{cat} = 0.079 \text{ s}^{-1}$, $K_m = 0.66 \text{ mM}$, and $k_{cat}/K_m = 120 \text{ M}^{-1} \text{ s}^{-1}$ in the presence of Ca^{2+} and $k_{cat} = 1.83 \times 10^{-3} \text{ s}^{-1}$, $K_m =$

Embryonic Blastula Protease 10 from Sea Urchin

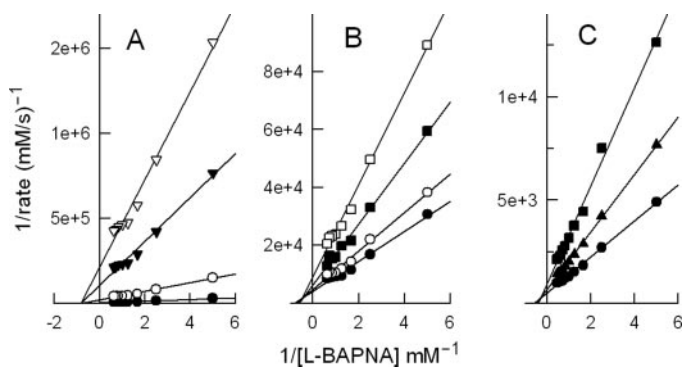


FIGURE 8. Inhibition of Zn-BP10 toward L-BAPNA hydrolysis in 50.0 mM HEPES, pH 7.5, 50.0 mM NaCl, 1.0 mM $\text{Ca}(\text{NO}_3)_2$ by 1,10-phenanthroline (A) and by Arg-NHOH (B). Inhibition of Cu-BP10 by Arg-NHOH is shown in C. Inhibitor concentrations are as follows from bottom to top: 0, 0.5, 1.0, and 2.0 mM (A); 0, 0.25, 0.5, and 1.0 mM (B); 0, 1.5, and 3.0 μM (C).

1.55 mM, and $k_{\text{cat}}/K_m = 1.18 \text{ M}^{-1} \text{ s}^{-1}$ in the absence of Ca^{2+} (Fig. 7B). As in gelatin hydrolysis by BP10, Ca^{2+} activates BP10 by lowering the activation energy and enhancing substrate binding, as reflected in the rate constants as discussed above. The higher k_{cat} and lower K_m values for gelatin hydrolysis than for BAPNA hydrolysis also indicate a higher affinity of gelatin than BAPNA binding to BP10. The ability to hydrolyze both substrates reflects the endopeptidase nature of BP10.

The pH profiles for BAPNA hydrolysis by Zn-BP10 (Fig. 6, B and E) compare well with those of gelatin, showing a bell-shaped curve that can be fitted to a double ionization process. The ionization constants also fall within the experimental range, yielding $\text{p}K_{a1} = 5.39$ and $\text{p}K_{a2} = 9.18$ for k_{cat} , and $\text{p}K_{a1} = 5.83$ and $\text{p}K_{a2} = 8.98$ for k_{cat}/K_m . Since the pH profile of k_{cat}/K_m can reveal the ionization status of the enzyme and/or the substrate, the significantly different $\text{p}K_{a2}$ values between gelatin and BAPNA during hydrolysis reflect that the substrates may be involved in the deprotonation process during catalysis. The nature of the general acid corresponding to $\text{p}K_{a2}$ cannot be revealed at this stage on the study of Zn-BP10 (however, see below regarding the study of Cu-BP10).

The inhibition of Zn-BP10 by the metal chelator 1,10-phenanthroline toward the hydrolysis of BAPNA at pH 7.5 shows a noncompetitive pattern and $K_i = 7.85 \mu\text{M}$, which is consistent with metal removal from metalloenzymes (Fig. 8A). The mixed type inhibition by Arg-NHOH is a good indication of a combination of specific interaction along with metal chelation afforded by the hydroxamate moiety. The mixed inhibition pattern for Arg-NHOH can be fitted to yield $K_{ic} = 0.20 \text{ mM}$ and $K_{iu} = 0.90 \text{ mM}$, representing the specific inhibition constant for the dissociation of the enzyme-inhibitor complex (EI) and the catalytic inhibition constant for the dissociation of the inhibitor from the enzyme-substrate-inhibitor complex (ESI), respectively (35).

Mechanistic Studies of the Copper Derivative of BP10 (Cu-BP10)—The spectroscopically inert Zn^{2+} ion in astacin and several other metallohydrolases offers a poor probe for the investigation of the metal coordination environment in the active site. Thus, the Zn^{2+} is frequently replaced with other spectroscopically active metal ions to afford derivatives that can offer detailed insight into the catalytic mechanisms and structure within the active site (36). The formation of the Cu^{2+} -substituted BP10 (Cu-BP10) is evident by the intense Tyr-to- Cu^{2+} LMCT at 454 nm, analogous to that in Cu^{2+} -astacin and Cu^{2+} -serralylin (24, 37). The activity of Cu-BP10 is considerably higher than Zn-BP10 in terms of k_{cat} (0.76 s^{-1}) and k_{cat}/K_m ($5430 \text{ M}^{-1} \text{ s}^{-1}$), reflecting a 960% increase in activity in terms of k_{cat} and 485% in terms of k_{cat}/K_m . This is a rather unusual characteristic of metal derivatives of Zn enzymes, since most Cu^{2+} derivatives of Zn^{2+} -enzymes are inactive

(36). Increased activity of a Cu^{2+} derivative has been observed in serralylin, another metzincin family member able to hydrolyze gelatin and BAPNA (24). Moreover, the relative proteolytic activity of Cu-BP10 toward gelatin hydrolysis is $\sim 20\%$ of that of the zinc derivative, which is also greater than many metal-substituted metallohydrolases previously reported (36).

Metal-centered hydrolysis relies on the Lewis acidity of metal ions, which can lower the $\text{p}K_a$ of metal-bound water molecules by greater than 10^7 -fold, generating a metal-hydroxide at neutral pH that can perform nucleophilic attack on the scissile peptide bond. The versatility of metal-centered hydrolysis has been widely demonstrated in synthetic Cu^{2+} model systems, which show proficient peptidase activities and phosphodiesterase activities (38, 39, 40). Conversely, Cu^{2+} derivatives of metallohydrolases are generally inactive or exhibit considerably lower activities (36, 41) despite the comparatively high Lewis acidity of Cu^{2+} . Few examples of metal-substituted metallohydrolases in the literature show considerable activation, with serralylin (24) and astacin (37) being the most significant representatives of metal-substituted metallohydrolases that are activated by Cu^{2+} . The poor activation of metallohydrolases observed in Cu^{2+} derivatives may be attributed to Jahn-Teller distortion, which can reduce the nucleophilicity of the metal-bound water if positioned in the axial coordination of the metal center. The ability to use Cu^{2+} as a viable probe for mechanistic studies is characteristic of the astacin family of metalloenzymes. It is noteworthy that the ligands found in the astacin family are a unique example of metal-phenolate coordination in metallohydrolases, wherein the coordinated Tyr plays a “switch-off” role in catalysis (24, 25) and may be involved in the unique Cu^{2+} activation observed in astacin family enzymes thus far characterized. Our analysis of BP10 is consistent with this mechanism of hydrolysis.

From analysis of kinetic parameters k_{cat} and K_m , there is an obvious requirement of the metal center for catalysis. K_m value for the hydrolysis of BAPNA by Cu-BP10 in the presence of Ca^{2+} (1.32 mM) is not significantly different from the zinc form (0.66 mM) when compared with the 960% increase in k_{cat} of Cu-BP10 relative to the native Zn-BP10. Once again, as previously discussed, a small change in K_m concomitant with a large increase in k_{cat} suggests a lowering of the activation energy and an increase in the affinity for the substrate to bind with the enzyme. The hyperactive Cu-BP10 suggests that the metal center must be involved in catalysis, most importantly in the turnover of the ES complexes to the product with a high k_{cat} value.

Electronic spectra of the Cu^{2+} derivative were used for the study of the metal coordination environment in the active site, despite the low concentrations available for BP10 (the protein precipitates at above 70 μM). Upon binding of Cu^{2+} during the refolding of BP10, a 20 μM sample can show significant LMCT in the visible range. Unfortunately, the d-d transition bands for tetragonally distorted octahedral Cu^{2+} have very low molar absorptivity values (on the order of $100 \text{ M}^{-1} \text{ cm}^{-1}$) and are too noisy to distinguish in the spectrum (Fig. 9). The intense absorption ($\epsilon = 1210 \text{ M}^{-1} \text{ cm}^{-1}$) at 454 nm is due to the tyrosinate-to- Cu^{2+} charge transfer transition as determined previously in Cu-astacin (37). This is further proof of an astacin-like active site structure for BP10.

The inhibition of Cu^{2+} and Zn^{2+} (see above) derivatives of BP10 by Arg-NHOH at pH 7.50 (Fig. 8) displays a mixed inhibition pattern as observed in serralylin (25), wherein the inhibitor is able to bind both the enzyme and the ES complex. The mixed type inhibition yields two different inhibition constants for the dissociation of the inhibitor from the EI and EIS complexes, $K_{ic} = 1.58 \mu\text{M}$ and $K_{iu} = 3.93 \mu\text{M}$, respectively. The significantly different inhibition constants for Zn-BP10 and Cu-BP10 are good evidence that the inhibitor binds directly to the metal

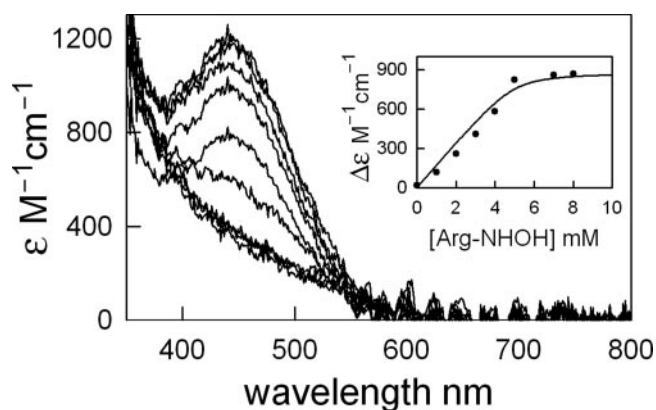
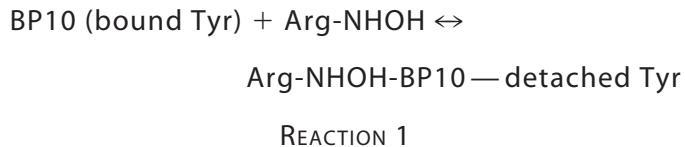


FIGURE 9. **Optical titration of Arg-NHOH to Cu-BP10.** The inset shows the decrease in the change of the molar absorptivity ($\Delta\epsilon$) as a function of [Arg-NHOH]. The data are fitted to a quadratic 1:1 ligand-binding relationship.

center in the active site. Mixed-type inhibition is often a good indicator of an alternative site for inhibitor and substrate binding in the *ES* complex to afford an *ESI* and *ESS* ternary complexes (35).

The influence on the LMCT centered at 454 nm can serve as an indicator for inhibitor binding directly to the metal center (Fig. 9). The quenching of the LMCT band upon inhibitor titration indicates that the metal-coordinated Tyr is detached upon inhibitor binding, a phenomenon observed in the studies of Cu-astacin (25, 42) and Cu-serralyisin (Fig. 9, inset) (24, 43). The gradual decrease of the LMCT intensity upon inhibitor binding can be described according to the following equilibrium, assuming that the binding of 1 eq of inhibitor per active site metal results in concomitant detachment of the coordinated Tyr.



Fitting the change in molar absorptivity ($\Delta\epsilon \text{ M}^{-1} \text{ cm}^{-1}$) as a function of [Arg-NHOH] to a quadratic ligand-binding function gives a poor fit (Fig. 9, inset), suggesting that the binding of the inhibitor does not follow a simple equilibrium. This is further supported by the mixed type inhibition observed toward the hydrolysis of BAPNA by BP10. The quadratic fit yields a dissociation constant of $2.2 \times 10^3 \text{ M}^{-1}$ for Arg-NHOH binding to Cu-BP10 at pH 8.5 (Fig. 9, inset). The specific inhibition constant K_{ic} for the inhibition of Cu-BP10 by Arg-NHOH at pH 7.5 can be converted into an apparent association constant of $6.33 \times 10^5 \text{ M}^{-1}$, which is greater than that at pH 8.5, indicating that the protonation of the metal-coordinated Tyr at lower pH assists the binding of Arg-NHOH to the metal center. This observation corroborates the pH-dependent activity profiles described below.

The kinetic parameters K_m , k_{cat} , and k_{cat}/K_m for the hydrolysis of BAPNA by Cu-BP10 were determined between pH values of 5.0 and 9.5 and exhibit bell-shaped curves (Fig. 6, C and F) that can be fitted to a two-ionization process of the catalysis to give $pK_{a1} = 5.48$ and $pK_{a2} = 7.98$ for the pH dependence of k_{cat} and $pK_{a1} = 5.83$ and $pK_{a2} = 7.99$ for the pH dependence of k_{cat}/K_m . The similar crystal structures of different metal derivatives of astacin (37) suggest that the coordination sphere of Zn^{2+} and Cu^{2+} derivatives of BP10 would be similar. The different ionization constants pK_{a1} and pK_{a2} between Zn- and Cu-BP10 are thus expected to be attributable to the different Lewis acidity of each metal but not due to different metal environments within the active site of BP10. The low pK_{a2} approaching pK_{a1} for Cu-BP10 causes a consider-

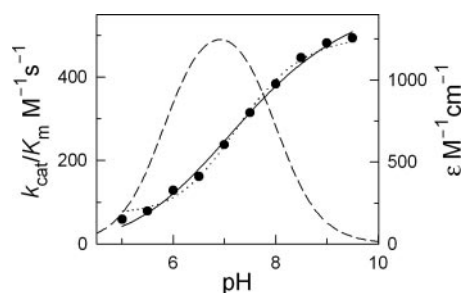


FIGURE 10. **The change in intensity of the LMCT transition of Cu-BP10 at 454 nm as a function of pH.** The fitting of the sigmoidal profile to a single deprotonation process is shown. The data are much better fitted to a two-ionization processes (solid trace) than to a single ionization process (dashed trace). The dashed bell-shaped curve is the best fit for the k_{cat}/K_m versus pH profile of Cu-BP10 from Fig. 5F.

able decrease in the catalytic efficiency, from the intrinsic value of $851 \text{ M}^{-1} \text{ s}^{-1}$ to the maximum fitted value of $580 \text{ M}^{-1} \text{ s}^{-1}$, which means that only 64% of Cu-BP10 is active at pH 7.0. Conversely, the intrinsic and fitted values for k_{cat}/K_m of Zn-BP10 differ only slightly with the intrinsic value of $120 \text{ M}^{-1} \text{ s}^{-1}$ and the fitted value of $125 \text{ M}^{-1} \text{ s}^{-1}$.

Ionizable groups must be coordinated or in very close proximity of the metal in the active site of a metalloenzyme to be influenced by the metal ion, as reflected by a change of pK_a values. In astacin, the crystal structure indicates that Tyr and a water molecule are bound to the metal center, with the latter hydrogen-bonded to the proximal Glu¹⁹¹. This framework generates the metal-bound nucleophile, metal-OH⁻...HOOC(Glu¹⁹¹), and proceeds via a general acid/general base mechanism wherein the coordinated water is sandwiched and activated by a Lewis acid (the active site metal) and a Lewis base (the carboxylate of Glu). This type of metal center has also been confirmed in other metallohydrolases, including serralyisin (24), thermolysin (44), matrilysin (45), and carboxypeptidase A (46). Since the native Zn^{2+} -BP10 is spectroscopically silent while Cu^{2+} -BP10 is active and spectroscopically rich, we utilized the Cu^{2+} derivative of BP10 to determine if a similar mechanism is utilized by this enzyme and to reveal the role of the coordinated Tyr in BP10.

The 454-nm Tyr(phenolate)-to- Cu^{2+} LMCT band in Cu-BP10 does not show full intensity at neutral and lower pH values ($\sim 150 \text{ M}^{-1} \text{ cm}^{-1}$ at pH 6.0 versus $1255 \text{ M}^{-1} \text{ cm}^{-1}$ at pH 8.5), indicating that they are pH-dependent. The charge transfer changes with pH in a sigmoidal manner (Fig. 10). Thus, the change can be described by the ionization of the coordinated Tyr²⁴⁹ and simultaneous binding to the active site Cu^{2+} to give $\epsilon_u = 109$ and $\epsilon_b = 1182 \text{ M}^{-1} \text{ cm}^{-1}$ and a pK_a value of 6.87, where ϵ_u and ϵ_b are the molar absorptivities due to the background and the copper-bound Tyr²⁴⁹. However, the data do not fit well to this single-ionization model (Fig. 10, dotted trace), and the pK_a value of 6.86 is not a close match to the k_{cat}/K_m pK_{a2} value of 7.99.

Since proposed models of astacin-type enzymes show that the Tyr side chain is hydrogen-bonded to the metal-coordinated water, the deprotonation of the phenolate moiety and subsequent binding to the active-site metal should be affected by the ionization of the coordinated water and reflected in the charge transfer intensities as previously described (24). The data are much better fitted to this two-ionization process with a fixed $pK_{a1} = 5.83$ (from the k_{cat}/K_m pH profile of Cu-BP10 (Fig. 5F) to afford $pK_{a2} = 7.42 \pm 0.15$, $\epsilon_u = 26 \pm 15$, $\epsilon_w = 591 \pm 33$, and $\epsilon_b = 1425 \text{ M}^{-1} \text{ cm}^{-1}$ (Fig. 9, solid trace), where ϵ_u , ϵ_w , and ϵ_b are molar absorptivities associated with the background and deprotonation of the coordinated water and the bound Tyr, respectively. Although the data can be reasonably fitted to the two-ionization process, the similar λ_{max} throughout the titration suggests that it is likely to have only one species that affords the LMCT instead of two, such as a tautomeric

Embryonic Blastula Protease 10 from Sea Urchin

equilibrium between the deprotonations of the water and the Tyr as previously proposed for serralsin (24). Taken together, our data are most consistently described as an ionization that results in the LMCT, initiated from a Tyr²⁴⁹-to-Cu²⁺ charge transfer.

Conclusion—BP10 is the first member of this enzyme family to be thoroughly characterized with kinetics and spectroscopic methods. The studies show that BP10 is a metallohydrolase with a hydrolytic mechanism consistent with other astacin-like proteases. The influence of Ca²⁺ on the hydrolysis of gelatin and BAPNA by BP10 implies that Ca²⁺ signaling may serve an important function in regulation of the proteolytic events in embryogenesis. The studies of the copper derivative support the Tyr switch and metal-centered mechanism previously proposed for astacin and serralsin, with the involvement of the metal-bound Tyr residue in catalysis. The understanding of the detailed mechanism of peptide hydrolysis by BP10 and revealing of the substrate specificity *in vivo* in future studies are important first steps in unraveling the proteolytic events during sea urchin embryogenesis.

Acknowledgments—We thank Thierry LePage and Christian Gache for providing a cDNA clone encoding BP10.

REFERENCES

- Bond, J. S., and Beynon, R. J. (1995) *Protein Sci.* **4**, 1247–1261
- Hooper, N. M. (ed) (1996) *Zinc Metalloproteases in Health and Disease*, pp. 23–46, Taylor and Francis, Bristol, PA
- Moehrlen, F., Hutter, H., and Zwilling, R. (2003) *Eur. J. Biochem.* **270**, 4909–4920
- Gomis-Rüth, F. X., Stöcker, W., Huber, H., Zwilling, R., and Bode, W. (1993) *J. Mol. Biol.* **229**, 945–968
- Lepage, T., Ghiglione, C., and Gache, C. (1992) *Development* **114**, 147–163
- Lepage, T., Ghiglione, C., and Gache, C. (1996) *Eur. J. Biochem.* **238**, 744–751
- Bode, W., Gomis-Rüth, F. X., Huber, R., Zwilling, R., and Stöcker, W. (1992) *Nature* **358**, 164–167
- Takahara, K., Brevard, R., Hoffman, G. F., Suzuki, N., and Greenspan, D. S. (1996) *Genomics* **34**, 157–165
- Wardle, F. C., Angerer, L. M., and Angerer, R. C. (1999) *Dev. Biol.* **206**, 63–72
- Appella, E., Weber, I. T., and Blasi, F. (1988) *FEBS Lett.* **231**, 1–4
- Uzel, M. I., Scott, I. C., Babakhanlou-Chase, H., Palamakumbura, A. H., Pappanos, W. N., Hong, H.-H., Greenspan, D. S., and Trackman, P. C. (2001) *J. Biol. Chem.* **276**, 22537–22543
- Butler, E., Hardin, J., and Benson, S. (1987) *Exp. Cell Res.* **173**, 174–182
- Wessel, G. M., and McClay, D. R. (1987) *Dev. Biol.* **121**, 149–165
- Hartigan, N., Garrigue-Antar, L., and Kadler, K. E. (2003) *J. Biol. Chem.* **278**, 18045–18049
- Sternlicht, M. D., and Werb, Z. (2001) *Cell. Dev. Biol.* **17**, 463–516
- Imai, K., Kusakabe, M., Sakakura, T., Nakanishiki, I., and Okada, Y. (1994) *FEBS Lett.* **352**, 216–218
- Vafa, O., and Nishioka, D. (1995) *Mol. Reprod. Dev.* **40**, 36–47
- Karakiulakis, G., Papakonstantinou, E., Maragoudakis, M. E., and Miseric, G. N. (1993) *J. Cell. Biochem.* **52**, 92–106
- Quigley, J. P., Braithwaite, R. S., and Armstrong, P. B. (1993) *Differentiation* **54**, 19–23
- Sharpe, C., and Robinson, J. J. (2001) *Biochem. Cell Biol.* **79**, 461–468
- Stöcker, W., Grams, F., Baumann, U., Reinemer, P., Gomis-Rüth, F. X., McKay, D. B., and Bode, W. (1995) *Protein Sci.* **4**, 823–840
- Kimura, E. (1994) *Prog. Inorg. Chem.* **41**, 443–491
- Kimura, E., and Koike, T. (1997) *Adv. Inorg. Chem.* **44**, 229–261
- Park, H. I., and Ming, L.-J. (2002) *J. Biol. Inorg. Chem.* **7**, 600–610
- Park, H. I., and Ming, L.-J. (1998) *J. Inorg. Biochem.* **72**, 57–62
- Chen, Y.-H., Yang, J. T., and Martinez, H. M. (1972) *Biochemistry* **11**, 4120–4131
- Murphy, G., and Crabbe, T. (1995) *Methods Enzymol.* **248**, 470–475
- Laemmli, U. K. (1970) *Nature* **227**, 680–685
- Grubb, J. D. (1994) *Methods Enzymol.* **235**, 602–606
- Friedman, M. (2004) *J. Agric. Food Chem.* **52**, 385–406
- Clark, E. D. B. (1998) *Biochem. Eng.* **9**, 157–163
- Sieron, A. L., Tretiakova, A., Segall, M. L., Lund-Katz, S., Khan, M. T., Li, S.-W., and Stöcker, W. (2000) *Biochemistry* **39**, 3231–3239
- Mayne, J., and Robison, J. J. (1998) *J. Cell. Biochem.* **71**, 546–558
- Calloway, C., Sharpe, C., and Robison, J. J. (2003) *Biochim. Biophys. Acta* **1621**, 67–75
- Cornish-Bowden, A. (1995) *Fundamentals of Enzyme Kinetics*, Portland Press, London
- Bertini, I., Gray, H. B., Lippard, S. J., Valentine, J. S., Bertini, I., and Luchinat, C. (eds) (1994) *Bioinorganic Chemistry*, pp. 37–106, University Science Books, Sausalito, CA
- Gomis-Rüth, F. X., Grams, F., Yiallourous, I., Nar, H., Küsthardt, U., Zwilling, R., Bode, W., and Stöcker, W. (1994) *J. Biol. Chem.* **269**, 17111–17117
- Hegg, E. L., and Burstyn, J. N. (2005) *Coord. Chem. Rev.* **173**, 133–165
- Frey, S. T., Murthy, N. N., Weintraub, S. T., Thompson, L. K., and Karlin, K. D. (1997) *Inorg. Chem.* **36**, 956–957
- Lykourinou-Tibbs, V., Bisht, K., and Ming, L.-J. (2005) *Inorg. Chim. Acta* **358**, 1247–1252
- Kimura, E., and Koike, T. (1997) *Adv. Inorg. Chem.* **44**, 229–261
- Grams, F., Dive, V., Yiotakis, A., Yiallourous, I., Vassiliou, S., Zwilling, R., Bode, W., and Stöcker, W. (1996) *Nat. Struct. Biol.* **3**, 671–675
- Baumann, U., Bauer, M., Letoffe, S., Delepelair, P., and Wandersman, C. (1995) *J. Mol. Biol.* **248**, 653–661
- Matthews, B. W. (1998) *Acc. Chem. Res.* **21**, 333–340
- Cha, J., and Auld, D. S. (1997) *Biochemistry* **36**, 16019–16024
- Christianson, D. W., and Lipscomb, W. N. (1989) *Acc. Chem. Res.* **22**, 62–69